Spontaneous Flows in Suspensions of Active Cyclic Swimmers

Tommaso Brotto[1] · **Denis Bartolo**[2] ·
David Saintillan[3]

Abstract Many swimming cells rely on periodic deformations to achieve locomotion. We introduce in this work a theoretical model and numerical simulations in order to elucidate the impact of these cyclic strokes on the emergence of mesoscale structures and collective motion in swimmer suspensions. The model extends previous kinetic theories for populations of identical swimmers to the case of self-propelled particles undergoing transitions between pusher and puller states, and is applied to quantify how the unsteadiness of the hydrodynamic velocity field, to which each swimmer population contributes, affects the onset and characteristics of spontaneous flows. A linear stability analysis reveals that the sign of the population-averaged dipole determines the stability of the uniform isotropic state, with suspensions dominated by pushers being subject to growing nematic bend fluctuations. Stochastic transitions, however, are also seen to provide an additional damping mechanism. To investigate the population dynamics above the instability threshold, we also perform direct particle

Communicated by Eva Kanso and David Saintillan.

✉ David Saintillan
   dstn@ucsd.edu

   Tommaso Brotto
   tommaso.brotto@lps.ens.fr

   Denis Bartolo
   denis.bartolo@ens-lyon.fr

[1] Laboratoire de Physique Statistique, École Normale Supérieure de Paris, 45, rue d'Ulm, 75005 Paris, France

[2] Laboratoire de Physique, École Normale Supérieure de Lyon, 46 allée d'Italie, 69007 Lyon, France

[3] Department of Mechanical and Aerospace Engineering, University of California San Diego, 9500 Gilman Drive, La Jolla, CA 92093, USA

simulations based on a slender-body model, where the growth or decay of the active power generated by the swimmers is found to be a robust measure of the structural and dynamical instability.

Keywords   Active suspensions · Collective motion · Kinetic theory · Hydrodynamic stability

Mathematics Subject Classification   92C05 · 92C17 · 76E99 · 76A05

1 Introduction

The emergence of collective motion and spontaneous flows is the hallmark of numerous active matter systems (Saintillan and Shelley 2013, 2015; Marchetti et al. 2013; Koch and Subramanian 2011) from bacterial suspensions (Dombrowski et al. 2004; Cisneros et al. 2011; Dunkel et al. 2013; Gachelin et al. 2014) to mixtures of biofilaments and molecular motors (Schaller et al. 2010; Sanchez et al. 2012; Keber et al. 2014; Gao et al. 2015) to populations of self-propelled colloids (Bricard et al. 2013, 2015) and shaken grains (Deseigne et al. 2010; Kumar et al. 2014). In all of these systems, interparticle interactions, whether hydrodynamic, electrostatic, or steric, tend to align neighboring particles and can drive large-scale coherent flows if they overcome randomizing processes such as thermal fluctuations or other sources of stochastic noise. Much attention has focused on suspensions of self-propelled particles, such as swimming microorganisms and autonomous catalytic micro-rods. In these suspensions, it has been argued that far-field hydrodynamic interactions resulting from the force dipole exerted by a self-propelled particle on its surroundings can drive long-wave instabilities that cause local nematic alignment, leading ultimately to collective motion and concentration fluctuations (Saintillan and Shelley 2008a, b; Subramanian and Koch 2009; Baskaran and Marchetti 2009). These theoretical models, which predict a critical concentration above which collective motion arises, are in qualitative agreement with experimental observations (Cisneros et al. 2011) as well as direct particle simulations based on various models (Saintillan and Shelley 2007; Hernandez-Ortiz et al. 2009; Saintillan and Shelley 2012) though it has been suggested that steric interactions also likely play a role in dense systems (Baskaran and Marchetti 2010; Ezhilan et al. 2013).

The key ingredient of these hydrodynamic theories is the intrinsic force dipole resulting from the swimming of an isolated particle. In the mean field, such dipoles amount to an additional stress contribution in the equations for the fluid motion (Hatwalne et al. 2004; Saintillan 2010), which modifies the effective viscosity of the suspension and can have a destabilizing effect. It is now widely admitted that the sign of the individual dipole strength σ determines the stability of homogeneous and isotropic suspensions: Extensile particles with $\sigma < 0$, also known as pushers, decrease the effective viscosity and are subject to instabilities, whereas contractile particles or pullers for which $\sigma > 0$ are not. The signature for this dipole is indeed observed in experiments, where flow fields around isolated swimming microorganisms were measured using particle-image velocimetry (Drescher et al. 2010; Guasto et al. 2010;

Drescher et al. 2011): In the case of neutrally buoyant microorganisms, the spatial decay of the velocity disturbance by one swimmer is indeed observed to go as r^{-2} in three dimensions, where r is the distance from the organism. Further, it was found that $\sigma < 0$ in suspensions of bacteria (Drescher et al. 2011), whereas $\sigma > 0$ in suspensions of swimming algae (Drescher et al. 2010; Guasto et al. 2010), thus supporting the theoretical predictions on suspension stability, as collective swirling motion in experiments is only observed in suspensions of the former. Another evidence of these oppositely signed dipoles is provided by rheological measurements, which indeed demonstrate decreased viscosities in bacterial suspensions (Sokolov and Aranson 2009; Gachelin et al. 2013) but enhanced viscosities in algae suspensions (Rafaï et al. 2010; Mussler et al. 2013).

Perhaps, one limitation of these previous models is the assumption that the very details of the swimming mechanisms at the individual level can be ignored. Instead, a unique and well-defined dipole strength σ that is steady and identical for all swimmers is suggested to fully dictate the large-scale structure and dynamics of the suspension. While this may apply to synthetic swimmers whose fabrication is well controlled, the situation is far from simple in biological suspensions. Indeed, biological swimmers are subject to phenotypic variations and one should rather expect a distribution of dipole strengths with a certain mean and variance: Is the stability in this case determined by the mean dipole strength, or do variations play a more intricate role? Furthermore, the assumption of a steady dipole for each particle is also known to be flawed: Time-resolved measurements on swimming algae (Guasto et al. 2010) indeed revealed the oscillatory nature of the flow they create, with a period equal to the duration of one swimming stroke (Goldstein 2015). Such oscillations are reflected in the dipole strength, which also varies in time and in fact even changes sign over the course of one stroke (Guasto et al. 2010). In other words, swimming algae periodically switch behavior between pusher and puller, even though their time-averaged dipole classifies them as pullers.

Such variations among swimming particles and cyclic dynamics of individual swimmers have not received much attention in the context of hydrodynamic theories and are the subject of the present work. Recent theoretical models have considered the impact of cyclic dynamics on phase synchronization in active suspensions (Fürthauer and Ramaswamy 2013; Leoni and Liverpool 2014) and suggest that synchronization may occur and drive new instabilities unobserved in phase-incoherent systems. Here, we do not address the effects of such synchronization, but rather focus on the stability of a suspension of swimmers whose cyclic dynamics are approximated as a Markov process in which individual particles switch back and forth between two states characterized by distinct swimming velocities and dipole strengths (e.g., pusher and puller states). The switching frequencies can be related to the mean residence time in each state and also determine the relative proportion of each population in the suspension. In the limit where these frequencies tend to zero while maintaining a fixed ratio, the model can also be applied to describe a mixture of two types of particles that do not switch type. As mechanisms for synchronization are excluded, the only coupling between the two populations of swimmers occurs through the hydrodynamic field they generate, which depends on the dipole strengths of both populations. We first analyze this system theoretically in Sect. 2 using a continuum model that extends previous

works on single populations (Saintillan and Shelley 2008b), and show that the stability in this system is simply determined by the concentration-weighted average of the dipole strengths, though the stochastic transitions between swimmer types are seen to provide an additional damping mechanism. These predictions are then tested in more detail using direct particle simulations of hydrodynamically interacting slender swimmers (Saintillan and Shelley 2012) in Sect. 3. We conclude in Sect. 4.

2 Theoretical Model

2.1 Fokker–Planck Description

We introduce two probability density functions $\Psi^+(\mathbf{r}, \mathbf{p}, t)$ and $\Psi^-(\mathbf{r}, \mathbf{p}, t)$ corresponding to two distinct swimmer states, such as puller and pusher. Conservation of probability is expressed by two coupled Fokker–Planck equations

$$\partial_t \Psi^+ + \nabla_{\mathbf{r}} \cdot (\dot{\mathbf{r}}^+ \Psi^+) + \nabla_{\mathbf{p}} \cdot (\dot{\mathbf{p}} \, \Psi^+) = -f_\pm \Psi^+ + f_\mp \Psi^-, \tag{1}$$

$$\partial_t \Psi^- + \nabla_{\mathbf{r}} \cdot (\dot{\mathbf{r}}^- \Psi^-) + \nabla_{\mathbf{p}} \cdot (\dot{\mathbf{p}} \, \Psi^-) = -f_\mp \Psi^- + f_\pm \Psi^+, \tag{2}$$

where transitions between the two states (with rates $f_\pm$ and $f_\mp$) are modeled on the right-hand side as a continuous-time Markov process. The average times spent by the particles in each state are given by $T_\pm = f_\pm^{-1}$ and $T_\mp = f_\mp^{-1}$, and a characteristic timescale for relaxation of fluctuations due to stochastic transitions is provided by $\langle T \rangle = (f_\pm + f_\mp)^{-1} = T_\pm T_\mp / (T_\pm + T_\mp)$, or half the harmonic mean of the average residence times for each state. The two distribution functions are related to the mean number density n as

$$\frac{1}{V} \int_V \int_\Omega [\Psi^+(\mathbf{r}, \mathbf{p}, t) + \Psi^-(\mathbf{r}, \mathbf{p}, t)] \, d\mathbf{p} \, d\mathbf{r} = n, \tag{3}$$

where V is the volume of the system and Ω denotes the unit sphere of orientations. In Eqs. (1)–(2), the translational flux velocities $\dot{\mathbf{r}}^\pm$ are modeled as

$$\dot{\mathbf{r}}^\pm = U_s^\pm \mathbf{p} + \mathbf{u}(\mathbf{r}, t) - D \nabla_{\mathbf{r}} \ln \Psi(\mathbf{r}, \mathbf{p}, t), \tag{4}$$

which accounts for swimming in the direction of $\mathbf{p}$ at a constant velocity $U_s^\pm$ (which need not be the same for both swimmer states), advection by the local flow field $\mathbf{u}(\mathbf{r}, t)$, and diffusion with isotropic and constant diffusivity D. The orientational velocity $\dot{\mathbf{p}}$ is the same for both populations and captures rotation and alignment by the flow according to Jeffery's equation, as well as rotational diffusion:

$$\dot{\mathbf{p}} = (\mathbf{I} - \mathbf{p}\mathbf{p}) \cdot \mathbf{T}(\mathbf{r}, t) \cdot \mathbf{p} - d \nabla_{\mathbf{p}} \ln \Psi(\mathbf{r}, \mathbf{p}, t). \tag{5}$$

Here, $\mathbf{T} = \gamma \mathbf{E} - \mathbf{W}$, where $\mathbf{E} = [\nabla_{\mathbf{r}}\mathbf{u} + \nabla_{\mathbf{r}}\mathbf{u}^\dagger]/2$ and $\mathbf{W} = [\nabla_{\mathbf{r}}\mathbf{u} - \nabla_{\mathbf{r}}\mathbf{u}^\dagger]/2$ are the rate-of-strain and rate-of-rotation tensors, respectively, with † denoting transposition. The Bretherton constant γ depends on the shape of the particle (Bretherton 1962),

with $\gamma = 0$ for an isotropic particle such as a sphere and $\gamma \approx 1$ for slender rod-like particles such as bacteria and many self-propelled catalytic micro-rods. Both swimmer types contribute to the fluid flow by exerting active stresses on their surroundings. The velocity $\mathbf{u}(\mathbf{r}, t)$ solves the Stokes equations

$$\nabla_{\mathbf{r}} \cdot \mathbf{u} = 0, \qquad -\eta \nabla_{\mathbf{r}}^2 \mathbf{u} + \nabla_{\mathbf{r}} q = \nabla_{\mathbf{r}} \cdot \boldsymbol{\Sigma}^a(\mathbf{r}, t), \tag{6}$$

where η is the shear viscosity of the fluid and q the local pressure. The active stress tensor $\boldsymbol{\Sigma}^a$ driving the flow is expressed as (Hatwalne et al. 2004; Saintillan 2010)

$$\boldsymbol{\Sigma}^a(\mathbf{r}, t) = \int_{\Omega} \left(\mathbf{pp} - \frac{\mathbf{I}}{3} \right) [\sigma^+ \Psi^+(\mathbf{r}, \mathbf{p}, t) + \sigma^- \Psi^-(\mathbf{r}, \mathbf{p}, t)] \, d\mathbf{p}, \tag{7}$$

where $\sigma^+ > 0$ and $\sigma^- < 0$ are the dipole strengths of pullers and pushers, respectively.

2.2 Moment Equations

To make analytical progress, we assume that departures from isotropy are small and approximate the distribution functions in terms of their first three moments (Baskaran and Marchetti 2009):

$$\Psi^{\pm}(\mathbf{r}, \mathbf{p}, t) \approx \frac{c^{\pm}(\mathbf{r}, t)}{4\pi} \left[1 + 3\mathbf{p} \cdot \mathbf{P}^{\pm}(\mathbf{r}, t) + \frac{15}{2} \mathbf{pp} : \mathbf{Q}^{\pm}(\mathbf{r}, t) \right]. \tag{8}$$

In this expression, $c^{\pm}$, $\mathbf{P}^{\pm}$, and $\mathbf{Q}^{\pm}$ denote the concentration, polarization, and nematic order parameter tensor of each population:

$$c^{\pm}(\mathbf{r}, t) = \int_{\Omega} \Psi^{\pm}(\mathbf{r}, \mathbf{p}, t) \, d\mathbf{p}, \tag{9}$$

$$\mathbf{P}^{\pm}(\mathbf{r}, t) = \frac{1}{c^{\pm}} \int_{\Omega} \mathbf{p} \, \Psi^{\pm}(\mathbf{r}, \mathbf{p}, t) \, d\mathbf{p}, \tag{10}$$

$$\mathbf{Q}^{\pm}(\mathbf{r}, t) = \frac{1}{c^{\pm}} \int_{\Omega} \left(\mathbf{pp} - \frac{\mathbf{I}}{3} \right) \Psi^{\pm}(\mathbf{r}, \mathbf{p}, t) \, d\mathbf{p}. \tag{11}$$

The truncation of the expansion in Eq. (8) implies a closure approximation for moments of order three and higher, which are assumed to be zero; note, however, that other closure relations yield qualitatively identical results. Using this approximation, one can derive closed hydrodynamic equations for the moments. For the population of pullers:

$$D_t c^+ = -U_s^+ \nabla \cdot (c^+ \mathbf{P}^+) + D \nabla^2 c^+ - f_{\pm} c^+ + f_{\mp} c^-, \tag{12}$$

$$D_t(c^+ \mathbf{P}^+) = -U_s^+ \left[\nabla \cdot (c^+ \mathbf{Q}^+) + \frac{1}{3} \nabla c^+ \right] + \frac{4}{5} c^+ \mathbf{T} \cdot \mathbf{P}^+ - \frac{1}{5} c^+ \mathbf{P}^+ \cdot \mathbf{T}$$
$$+ D \nabla^2 (c^+ \mathbf{P}^+) - 2d c^+ \mathbf{P}^+ - f_{\pm} c^+ \mathbf{P}^+ + f_{\mp} c^- \mathbf{P}^-, \tag{13}$$

$$D_t(c^+\mathbf{Q}^+) = \frac{1}{5}U_s^+ \left[\frac{2}{3}\nabla \cdot (c^+\mathbf{P}^+)\mathbf{I} - \nabla(c^+\mathbf{P}^+) - \nabla(c^+\mathbf{P}^+)^\dagger \right]$$
$$+ \frac{1}{5}c^+(\mathbf{T} + \mathbf{T}^\dagger) - \frac{2}{7}c^+(\mathbf{T} : \mathbf{Q}^+)\mathbf{I} - \frac{1}{7}c^+\mathbf{Q}^+ \cdot \left(2\mathbf{T} - 5\mathbf{T}^\dagger \right)$$
$$- \frac{1}{7}c^+ \left(2\mathbf{T} - 5\mathbf{T}^\dagger \right) \cdot \mathbf{Q}^+ + D\nabla^2(c^+\mathbf{Q}^+) - 6dc^+\mathbf{Q}^+$$
$$- f_\pm c^+\mathbf{Q}^+ + f_\mp c^-\mathbf{Q}^-, \tag{14}$$

where $D_t \equiv \partial_t + \mathbf{u} \cdot \nabla$ is the material derivative. In these equations and below, it is implicit that ∇ denotes the gradient operator with respect to position $\mathbf{r}$, as the moments do not depend on $\mathbf{p}$. Similar equations are easily written for the population of pushers. The analytic expression for the tensor $\mathbf{T}$ follows from Eq. (6), where the active stress tensor can be recast in terms of the two dipole strengths, concentrations, and nematic order parameter tensors: $\mathbf{\Sigma}^a = \sigma^+c^+\mathbf{Q}^+ + \sigma^-c^-\mathbf{Q}^-$.

2.3 Linear Stability Analysis

In order to address the impact of conformational changes on the onset of spontaneous flows, we analyze the linear stability of the quiescent uniform and isotropic state. The concentration of each species in the base state is

$$c_0^+ = \frac{f_\mp}{f_\mp + f_\pm}n, \quad c_0^- = \frac{f_\pm}{f_\mp + f_\pm}n, \tag{15}$$

with zero polarization and nematic alignment, as well as zero flow. We introduce the excess fraction $\Delta\phi$ of pullers with respect to pushers as

$$\Delta\phi = \frac{1}{n}\left(c_0^+ - c_0^-\right) = \frac{f_\mp - f_\pm}{f_\mp + f_\pm}. \tag{16}$$

Note that $\Delta\phi \in [-1, 1]$, with the two extreme values corresponding to suspensions of all pushers or pullers, respectively. Equations (12)–(14) are easily linearized about the base state, yielding the simpler system

$$\partial_t\delta c^+ = -U_s^+c_0^+\nabla \cdot \delta\mathbf{P}^+ + D\nabla^2\delta c^+ - f_\pm\delta c^+ + f_\mp\delta c^-, \tag{17}$$
$$\partial_t(c_0^+\delta\mathbf{P}^+) = -U_s^+ \left[c_0^+\nabla \cdot \delta\mathbf{Q}^+ + \frac{1}{3}\nabla\delta c^+ \right]$$
$$+ Dc_0^+\nabla^2\delta\mathbf{P}^+ - 2dc_0^+\delta\mathbf{P}^+ - f_\pm c_0^+\delta\mathbf{P}^+ + f_\mp c_0^-\delta\mathbf{P}^-, \tag{18}$$
$$\partial_t(c_0^+\delta\mathbf{Q}^+) = \frac{U_s^+c_0^+}{5} \left[\frac{2}{3}(\nabla \cdot \delta\mathbf{P}^+)\mathbf{I} - \nabla\delta\mathbf{P}^+ - (\nabla\delta\mathbf{P}^+)^\dagger \right] + \frac{1}{5}c_0^+(\mathbf{T} + \mathbf{T}^\dagger)$$
$$+ Dc_0^+\nabla^2\delta\mathbf{Q}^+ - 6dc_0^+\delta\mathbf{Q}^+ - f_\pm c_0^+\delta\mathbf{Q}^+ + f_\mp c_0^-\delta\mathbf{Q}^-, \tag{19}$$

where variables preceded by a δ denote perturbations with respect to the base state. In an unbounded domain, one can consider plane-wave perturbations of the form

$$\{\delta c^{\pm}, \delta \mathbf{P}^{\pm}, \delta \mathbf{Q}^{\pm}\} = \{\widetilde{c}^{\pm}, \widetilde{\mathbf{P}}^{\pm}, \widetilde{\mathbf{Q}}^{\pm}\} \exp(i\mathbf{k}\cdot\mathbf{r} + \lambda t), \tag{20}$$

and without loss of generality, we choose a coordinate system in which the wave vector is aligned with the x-axis: $\mathbf{k} = k\hat{\mathbf{x}}$. Inserting Eq. (20) into (17)–(19), we easily arrive at an algebraic eigenvalue problem for the wave amplitudes:

$$\lambda\widetilde{c}^{+} = -U_s^{+}c_0^{+}ik\,\widetilde{P}_x^{+} - f_{\pm}\widetilde{c}^{+} + f_{\mp}\widetilde{c}^{-}, \tag{21}$$

$$\lambda\widetilde{P}_x^{+} = -U_s^{+}ik\left(\widetilde{Q}_{xx}^{+} + \frac{1}{3}\frac{\widetilde{c}^{+}}{c_0^{+}}\right) - (2d + f_{\pm})\widetilde{P}_x^{+} + f_{\pm}\widetilde{P}_x^{-}, \tag{22}$$

$$\lambda\widetilde{P}_y^{+} = -U_s^{+}ik\,\widetilde{Q}_{xy}^{+} - (2d + f_{\pm})\widetilde{P}_y^{+} + f_{\pm}\widetilde{P}_y^{-}, \tag{23}$$

$$\lambda\widetilde{P}_z^{+} = -U_s^{+}ik\,\widetilde{Q}_{xz}^{+} - (2d + f_{\pm})\widetilde{P}_z^{+} + f_{\pm}\widetilde{P}_z^{-}, \tag{24}$$

$$\lambda\widetilde{Q}_{xx}^{+} = -\frac{4}{15}U_s^{+}ik\,\widetilde{P}_x^{+} - (6d + f_{\pm})\widetilde{Q}_{xx}^{+} + f_{\pm}\widetilde{Q}_{xx}^{-}, \tag{25}$$

$$\lambda\widetilde{Q}_{yy}^{+} = \frac{2}{15}U_s^{+}ik\,\widetilde{P}_y^{+} - (6d + f_{\pm})\widetilde{Q}_{yy}^{+} + f_{\pm}\widetilde{Q}_{yy}^{-}, \tag{26}$$

$$\lambda\widetilde{Q}_{xy}^{+} = -\frac{1}{5}U_s^{+}ik\,\widetilde{P}_y^{+} - \left(6d + f_{\pm} + \frac{\gamma c_0^{+}\sigma^{+}}{5\eta}\right)\widetilde{Q}_{xy}^{+} + \left(f_{\pm} - \frac{\gamma c_0^{-}\sigma^{-}}{5\eta}\right)\widetilde{Q}_{xy}^{-}, \tag{27}$$

$$\lambda\widetilde{Q}_{yz}^{+} = -(6d + f_{\pm})\widetilde{Q}_{yz}^{+} + f_{\pm}\widetilde{Q}_{yz}^{-}. \tag{28}$$

For brevity, we have set $D = 0$, as the only effect of translational diffusion is to offset the eigenvalues by $-Dk^2$. Note that the equation for $\widetilde{Q}_{xz}^{+}$ is identical to that for $\widetilde{Q}_{xy}^{+}$ and that equations for the remaining components of the nematic tensor need not be specified as they can be inferred from the above using symmetry and tracelessness. Similar equations for the population of pushers are also readily obtained. In deriving Eq. (27), we have made use of the Fourier solution of the Stokes Eq. (6):

$$\widetilde{\mathbf{u}} = \frac{i}{\eta k}(\mathbf{I} - \hat{\mathbf{x}}\hat{\mathbf{x}})\cdot\left(\sigma^{+}c_0^{+}\widetilde{\mathbf{Q}}^{+} + \sigma^{-}c_0^{-}\widetilde{\mathbf{Q}}^{-}\right)\cdot\hat{\mathbf{x}}. \tag{29}$$

The eigenvalue problem (21)–(28) can be solved for λ, the real part of which determines the growth rate. Before solving the full system, we gain physical insight by analyzing the long-wave limit of $k \to 0$. In this case, couplings between variables vanish and simple closed-form solutions can be obtained for the eigenvalues, which come in pairs:

$$\widetilde{c}: \quad \lambda = 0 \ ; \ -(f_{\pm} + f_{\mp}), \tag{30}$$

$$\widetilde{P}_x, \widetilde{P}_y, \widetilde{P}_z: \quad \lambda = -2d \ ; \ -2d - (f_{\pm} + f_{\mp}), \tag{31}$$

$$\widetilde{Q}_{xx}, \widetilde{Q}_{yy}, \widetilde{Q}_{yz}: \quad \lambda = -6d \ ; \ -6d - (f_{\pm} + f_{\mp}), \tag{32}$$

$$\widetilde{Q}_{xy}: \quad \lambda = -6d - \frac{\gamma n}{5\eta}\langle\sigma\rangle \ ; \ -6d - (f_{\pm} + f_{\mp}). \tag{33}$$

These eigenvalues are all real in the long-wave limit and define the growth rates of the corresponding eigenmodes. In particular, we find that all perturbation variables are damped as a result of rotational diffusion (with diffusivity d) and of the stochastic transitions between puller and pusher states, with relaxation time $\langle T \rangle = (f_\pm + f_\mp)^{-1}$. In the case of $\widetilde{Q}_{xy}$, which describes nematic bend modes in the system, an additional eigenvalue arises due to hydrodynamic interactions and involves the population-averaged dipole:

$$\langle \sigma \rangle = \frac{1}{n} \left(c_0^+ \sigma^+ + c_0^- \sigma^- \right). \tag{34}$$

Since σ^+ and σ^- have opposite signs, the average dipole can be either positive or negative depending on the proportion of pushers vs pullers in the system. In the simple case where $\sigma^+ = -\sigma^- = |\sigma|$, it is simply given by $\langle \sigma \rangle = \Delta \phi |\sigma|$. From Eq. (33), we see that this mode can become unstable if

$$\langle \sigma \rangle \leq \sigma_c = -\frac{30 d \eta}{\gamma n}, \tag{35}$$

which implies a suspension dominated by pushers ($\Delta \phi < 0$). As anticipated, this instability competes against the randomizing effect of rotational diffusion. In the unstable case, an estimate for the characteristic time τ for growth of the nematic bend modes is provided by the inverse growth rate:

$$\tau = \left(\frac{\gamma n}{6\eta} |\langle \sigma \rangle| - 6d \right)^{-1} = \left(\frac{\gamma n |\sigma|}{6\eta} |\Delta \phi| - 6d \right)^{-1}. \tag{36}$$

In the limit of weak diffusion relevant to the simulations of Sect. 3, it defines a viscous active timescale τ_a that is inversely proportional to the average magnitude of active stresses in the suspension:

$$\tau \approx \tau_a = \frac{6\eta}{\gamma n |\sigma|} |\Delta \phi|^{-1}. \tag{37}$$

At finite wavelengths ($k > 0$), advection due to swimming leads to additional couplings between modes through the terms involving self-propulsion, i.e., $U_s^\pm$, in Eqs. (21)–(28). The structure of this system suggests scaling times with the stochastic timescale $\langle T \rangle$. Dimensional analysis then reveals that the dimensionless growth rate $\lambda \langle T \rangle$ (corrected for translational diffusion) is only a function of $U_s^\pm k \langle T \rangle$, $\Delta \phi$, $d \langle T \rangle$, and $\tau_a / \langle T \rangle$. Some of these dependences are probed more precisely in Fig. 1, showing numerical solutions of the eigenvalue problem (21)–(28). The only effect of increasing wavenumber is to reduce the magnitude of the maximum growth rate if all other parameters are kept fixed. The maximum growth rate, however, asymptotes to a constant positive value in the unstable regime as $U_s k \langle T \rangle \to \infty$. This high-wavenumber instability, which is in fact regularized by translational diffusion, is really an artifact of the truncation of Eq. (8) after three moments; interactions between higher moments
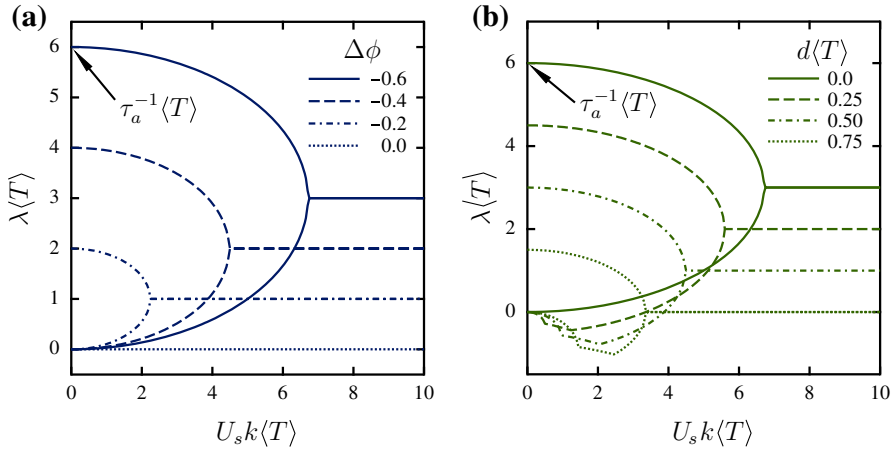
Fig. 1 Unstable eigenvalues in the numerical solution of the eigenvalue problem (21)–(28). Both *plots* show the dimensionless growth rate $\lambda\langle T\rangle$ vs dimensionless wavenumber $U_s k\langle T\rangle$: **a** effect of $\Delta\phi$ (in the absence of rotational diffusion), and **b** effect of the rotational diffusivity $d\langle T\rangle$ (for $\Delta\phi = -0.6$). In both plots, we have assumed $D = 0$ (no translational diffusion) and that pushers and pullers swim at the same speed U_s

in models based on the full Fokker–Planck equations are known to cause stabilization above a critical wavenumber k_c (Saintillan and Shelley 2008b; Hohenegger and Shelley 2010). The effect of $\Delta\phi$ is described in Fig. 1a, where instability is only found in suspensions dominated by pushers ($\Delta\phi < 0$), and increasing $\Delta\phi$ towards 0 stabilizes the system by decreasing the maximum growth rate according to (36). The stabilizing effect of rotational diffusion, also described by that equation, is shown in Fig. 1b and affects all wavenumbers equally. Furthermore, our numerical results suggest that differences in the swimming speeds U_s^+ and U_s^- of pullers and pushers only have a minor influence on the stability.

We conclude from this linearized hydrodynamic theory that a suspension of swimmers undergoing cyclic changes in their conformation obeys the same physics as a mixture of pushers and pullers, with a proportion set by the transition rates between the two states. Isotropic suspensions composed at all times of a larger fraction of pushers are prone to a long-wavelength instability inducing orientational nematic ordering on all scales.

3 Numerical Simulations

In order to test these theoretical predictions and gain insight into the nonlinear regime where the bending instability is fully developed, we use direct particle simulations based on the slender-body model of Saintillan and Shelley (2007, 2012). Briefly, the model describes swimmers as slender rigid rods that propel themselves by exerting a prescribed shear stress distribution over half of their length; the other half is subject to the usual no-slip condition for viscous flow. By prescribing this stress on the anterior or

posterior half of the swimmers, pullers and pushers can both be simulated. Hydrodynamic interactions between swimmers are calculated in a periodic cubic domain using an integral representation of the flow field based on Green's functions and are evaluated efficiently using a smooth particle-mesh Ewald algorithm (Saintillan et al. 2005). Transitions between puller and pusher states are modeled using a discrete implementation of a continuous-time Markov chain, in which the duration each swimmer remains in a given state is drawn from an exponential distribution with a mean equal to the average residence time in that state. We do not account for translational or rotational diffusion in the equations of motion, which are purely deterministic; the chaotic nature of hydrodynamic interactions between swimmers, however, leads to diffusive random walks at long times. Details on the numerical implementation are provided elsewhere (Saintillan and Shelley 2012).

In this section, variables are made dimensionless based on the particle length ℓ and swimming speed U_s, which are taken to be the same for pushers and pullers. In all the simulations shown here, a total number of $N = 8000$ particles is present in a cubic periodic domain of unit width 10. Pushers and pullers exert constant dipoles of opposite magnitudes: $\sigma^- = -\sigma^+$, so that based on the theoretical predictions, we expect the sign of $\Delta\phi$ to determine the stability and behavior of the suspension. This is indeed the case in our simulations, as illustrated in Fig. 2 showing typical particle distributions and velocity fields in two suspensions with $\Delta\phi = \pm 0.75$. In suspensions dominated by pullers in Fig. 2a, the particle configurations remain random and isotropic on all scales, with no clear particle alignment or density fluctuations. As a result, the correlation length of the velocity field is of the order of the particle size and is simply the result of the superposition of single-particle flow fields. On the other hand, a suspension dominated by pushers is shown in Fig. 2b and exhibits large coherent dynamical structures with clear local nematic alignment, in agreement with the prediction of Sect. 2 where the instability was found to pertain to the nematic order parameter $\widetilde{Q}_{xy}$; strong density fluctuations are also visible. Correspondingly, the flow field in the suspensions is strong and correlated on the scale of the system, with the presence of intense jets and vortices that fluctuate in time. Qualitatively, the dynamics observed in Fig. 2 is very similar to that reported in suspensions of either pushers or pullers in previous studies (Saintillan and Shelley 2007, 2012).

A quantitative measure of instability is provided by the active power $P(t)$ generated by the swimming particles. Within the continuum model, it is easily defined from a mechanical energy balance where it is found to balance viscous dissipation in the fluid (Saintillan and Shelley 2008b):

$$P(t) = -\int_V [\mathbf{E}(\mathbf{r}, t) : \mathbf{\Sigma}^a(\mathbf{r}, t)] \, d\mathbf{r} = 2\eta \int_V [\mathbf{E}(\mathbf{r}, t) : \mathbf{E}(\mathbf{r}, t)] \, d\mathbf{r}. \qquad (38)$$

As discussed by Saintillan and Shelley (2015), this active power in the linear regime is also a measure of the energy of the unstable nematic bend modes in the system and is therefore an appropriate measure of instability: In a suspension dominated by pushers, it is expected to show short-time exponential growth at a rate of $2\lambda \propto |\Delta\phi|^{-1}$. Conversely, it is expected to decay in suspensions dominated by pullers. In discrete simulations, the total active power is calculated more directly as
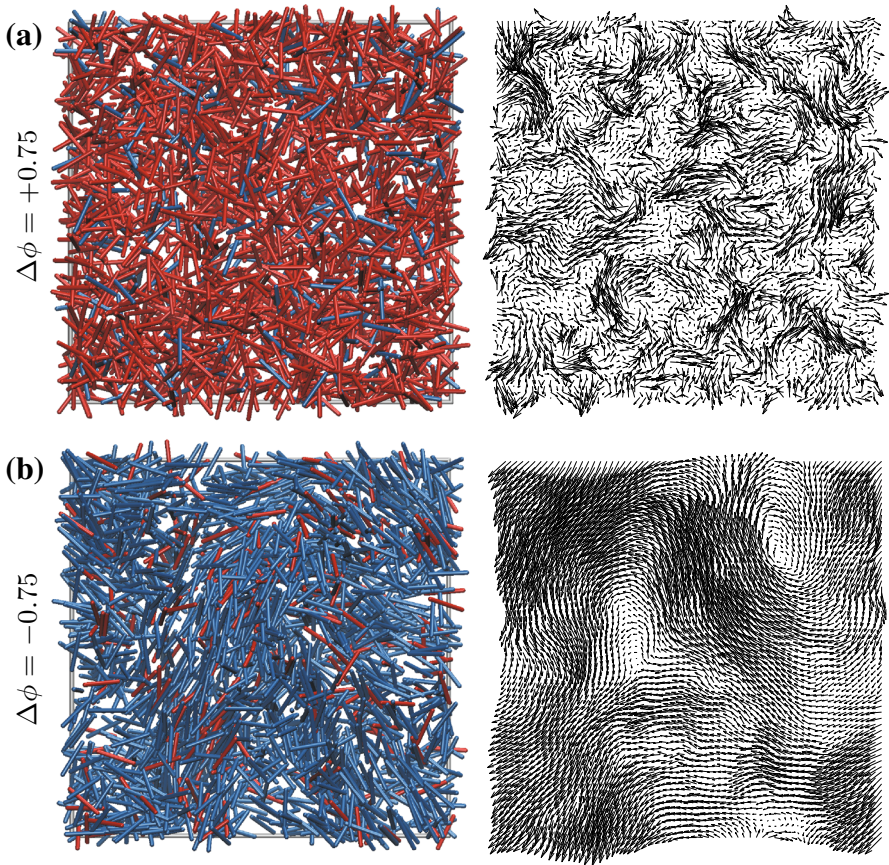
Fig. 2 *Left panel* particle distributions in simulations of $N = 8000$ pushers and pullers at $\langle T \rangle = 5$, for two different excess fractions: **a** $\Delta\phi = 0.75$ (puller-dominated), and **b** $\Delta\phi = -0.75$ (pusher-dominated). Colors correspond to instantaneous swimmer type: *red* = puller, *blue* = pusher. *Right panel* corresponding fluid velocity fields in a plane across the suspension

$$P(t) = \sum_{i=1}^{N} \int_{-\ell/2}^{\ell/2} \mathbf{f}_i(s_i) \cdot \mathbf{u}(s_i)\, ds_i, \tag{39}$$

where $\mathbf{f}_i$ is the linear force distribution along the centerline of particle i and contains contributions from swimming as well as hydrodynamic interactions. Note that it includes a constant single-particle contribution P_0 that is not present in the continuum definition of Eq. (38).

This discrete power was calculated numerically, and Fig. 3a shows the normalized power $P(t)/P_0 - 1$ vs time for different values of $\Delta\phi$ ranging from -1.0 (all pushers) to $+1.0$ (all pullers). The trends we observe are in agreement with the stability analysis: The normalized power is positive and is found to grow in suspensions dominated by pushers for which $\Delta\phi < 0$; on the other hand, it is found to decrease below the single-particle value in suspensions dominated by pullers. When $\Delta\phi = 0$ (equal amounts
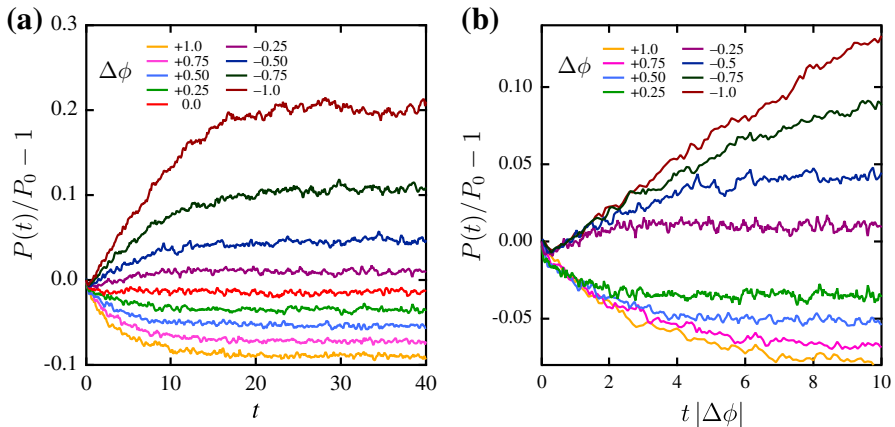
Fig. 3 **a** Normalized active power $P(t)/P_0 - 1$ in suspensions with different excess fractions $\Delta\phi$ plotted vs (**a**) time t, and **b** rescaled time $t\,|\Delta\phi|$. All simulations were performed with the same total number of particles $N = 8000$ and a mean residence time of $\langle T \rangle = 5$

Fig. 4 Normalized steady-state power $P_{ss}/P_0 - 1$ vs excess fraction of pullers $\Delta\phi$ in suspensions of $N = 8000$ swimmers, for different values of the mean residence time $\langle T \rangle$. The limit of $\langle T \rangle \to \infty$ describes a mixture of pushers and pullers that do never switch type
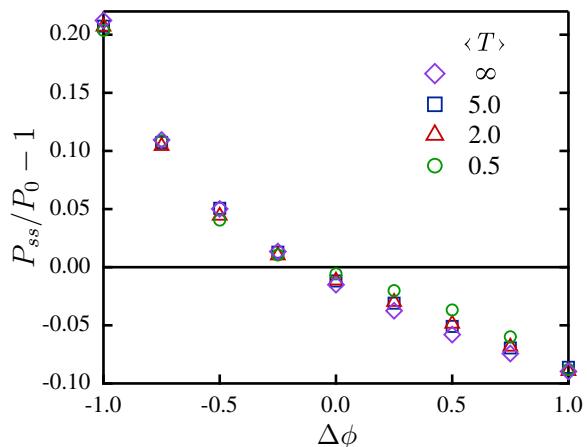
of pushers and pullers), the power remains nearly constant at a value close to the single-particle contribution, suggesting a neutrally stable system. Regardless of the value of $\Delta\phi$, the power always asymptotes to a finite steady-state value P_{ss} which is largest in the most unstable suspensions. As discussed above, the timescale for growth or decay of $P(t)$ is expected to be 2λ, which is proportional to $|\Delta\phi|^{-1}$ in the absence of rotational diffusion. This prediction is tested more precisely in Fig. 3b, where the data of Fig. 3a are now plotted vs a rescaled time $t\,|\Delta\phi|$: As expected, all the curves collapse at short times onto either of two linear profiles depending on the sign of $\Delta\phi$, in agreement with the linear stability results.

The dependence of the normalized steady-state power on the excess fraction $\Delta\phi$ is shown in Fig. 4 for different values of $\langle T \rangle$. As expected, we find that the steady-state power is positive in suspensions with $\Delta\phi < 0$ and negative otherwise. A small negative

value is observed when $\Delta\phi = 0$, which indicates a weak damping of fluctuations ($\lambda <$ 0) even when there are equal numbers of pushers and pullers: This trend is consistent with the stabilizing influence of finite system size as predicted by the stability analysis (Fig. 1). The steady-state power is seen to be only very weakly affected by the mean residence time $\langle T \rangle$, even in the limit of $\langle T \rangle \to \infty$, which describes a mixture of pushers and pullers that do never switch type. The weak variations observed (slightly weaker steady-state power for lower values of $\langle T \rangle$) again agree with the stability results of (30)–(33), where $\lambda = -\langle T \rangle = -(f_{\pm} + f_{\mp})^{-1}$ was found to be a stable eigenvalue.

4 Conclusions

Using a simple kinetic model and particle simulations, we have analyzed the stability and the onset of spontaneous flows in suspensions of self-propelled particles that cyclically switch between two modes of locomotion. The main finding of this work is that the stability of such suspensions is dictated primarily by the sign of the population-averaged dipole $\langle \sigma \rangle$ in the system, with suspensions dominated by pushers ($\langle \sigma \rangle < 0$) being subject to the growth of unstable nematic bend modes. In this sense, these mixtures behave very much like suspensions of identical swimmers that do not switch type but are characterized by an effective dipole strength given by $\langle \sigma \rangle$. The only other noticeable effect of the stochastic transitions is to provide a new mechanism for damping of fluctuations, with a characteristic timescale given by the mean residence time $\langle T \rangle$; this additional damping, however, was observed to be weak in particle simulations.

This study was motivated by the realization that biological swimmers are subject to phenotypic variations and are also known to perform cyclic swimming strokes during which their behavior as pushers or pullers changes periodically (Guasto et al. 2010). In this respect, the validity of our model in which transitions between states follow a Markov chain may be put in question, as the distribution of times spent in each state is exponential in our model as opposed to being narrowly centered on the period of oscillation of the swimming motions. However, the weak dependence of our simulation results on $\langle T \rangle$, which extends even to the limit of $\langle T \rangle \to \infty$, suggests that the role played by the population-average dipole would likely be the same even with a more realistic description of the quasi-periodic motions. As a final comment, we recall that mechanisms for hydrodynamic synchronization between swimmers were not included in our model, though synchronization has been shown in other works (Fürthauer and Ramaswamy 2013; Leoni and Liverpool 2014) to be a driver of additional instabilities.

References

Baskaran, A., Marchetti, M. C.: Nonequilibrium statistical mechanics of self-propelled hard rods. J. Stat. Mech.: Theor. Exp. P04019 (2010)
Baskaran, A., Marchetti, M.C.: Statistical mechanics and hydrodynamics of bacterial suspensions. Proc. Natl. Acad. Sci. USA **106**, 15567 (2009)

Bretherton, F.P.: The motion of rigid particles in a shear flow at low Reynolds number. J. Fluid Mech. **14**, 284 (1962)

Bricard, A., Caussin, J.-B., Das, D., Savoie, C., Chikkadi, V., Shitara, K., Chepizhko, O., Peruani, F., Saintillan, D., Bartolo, D.: Emergent vortices in populations of colloidal rollers. Nature Comm. (2015, to appear)

Bricard, A., Caussin, J.-B., Desreumaux, N., Dauchot, N., Bartolo, D.L.: Emergence of macroscopic directed motion in populations of motile colloids. Nature **503**, 95 (2013)

Cisneros, L.H., Kessler, J.O., Ganguly, S., Goldstein, R.E.: Dynamics of swimming bacteria: transition to directional order at high concentration. Phys. Rev. E **83**, 061907 (2011)

Deseigne, J., Dauchot, O., Chaté, H.: Collective motion of vibrated polar disks. Phys. Rev. Lett. **105**, 098001 (2010)

Dombrowski, C., Cisneros, L., Chatkaew, S., Goldstein, R.E., Kessler, J.O.: Self-concentration and large-scale coherence in bacterial dynamics. Phys. Rev. Lett. **93**, 098103 (2004)

Drescher, K., Goldstein, R.E., Michel, N., Polin, M., Tuval, I.: Direct measurement of the flow field around swimming microorganisms. Phys. Rev. Lett. **105**, 168101 (2010)

Drescher, K., Dunkel, J., Cisneros, L.H., Ganguly, S., Goldstein, R.E.: Fluid dynamics and noise in bacterial cell-cell and cell-surface scattering. Proc. Natl. Acad. Sci. USA **108**, 10940 (2011)

Dunkel, J., Heidenreich, S., Drescher, K., Wensink, H.H., Bär, M., Goldstein, R.E.: Fluid dynamics of bacterial turbulence. Phys. Rev. Lett. **110**, 228102 (2013)

Ezhilan, B., Shelley, M.J., Saintillan, D.: Instabilities and nonlinear dynamics of concentrated active suspensions. Phys. Fluids **25**, 070607 (2013)

Fürthauer, S., Ramaswamy, S.: Phase-synchronized state of oriented active fluids. Phys. Rev. Lett. **111**, 238102 (2013)

Gachelin, J., Miño, G., Berthet, H., Lindner, A., Rousselet, A., Clément, E.: Non-Newtonian viscosity of *Escherichia coli* suspensions. Phys. Rev. Lett. **110**, 268103 (2013)

Gachelin, J., Rousselet, A., Lindner, A., Clément, E.: Collective motion in an active suspension of *Escherichia coli* bacteria. New J. Phys. **16**, 025003 (2014)

Gao, T., Blackwell, R., Glaser, M.A., Betterton, M.D., Shelley, M.J.: Multiscale polar theory of microtubule and motor-protein assemblies. Phys. Rev. Lett. **114**, 048101 (2015)

Goldstein, R.E.: Green algae as model organisms for biological fluid dynamics. Annu. Rev. Fluid Mech. **47**, 353 (2015)

Guasto, J.S., Johnson, K.A., Gollub, J.P.: Oscillatory flows induced by microorganisms swimming in two dimensions. Phys. Rev. Lett. **105**, 168102 (2010)

Hatwalne, Y., Ramaswamy, S., Rao, M., Aditi Simha, R.: Rheology of active-particle suspensions. Phys. Rev. Lett. **92**, 118101 (2004)

Hernandez-Ortiz, J.P., Underhill, P.T., Graham, M.D.: Dynamics of confined suspensions of swimming particles. J. Phys. Condens. Matt. **21**, 204107 (2009)

Hohenegger, C., Shelley, M.J.: Stability of active suspensions. Phys. Rev. E **81**, 046311 (2010)

Keber, F.C., Loiseau, E., Sanchez, T., DeCamp, S.H., Giomi, L., Bowick, M.J., Marchetti, M.C., Dogic, Z., Bausch, A.R.: Topology and dynamics of active nematic vesicles. Science **345**, 6201 (2014)

Koch, D.L., Subramanian, G.: Collective hydrodynamics of swimming microorganisms: living fluids. Annu. Rev. Fluid Mech. **43**, 637 (2011)

Kumar, N., Soni, H., Ramaswamy, S., Sood, A.K.: Flocking at a distance in active granular matter. Nature Comm. **5**, 4688 (2014)

Leoni, M., Liverpool, T.B.: Synchronization and liquid crystalline order in soft active fluids. Phys. Rev. Lett. **112**, 148104 (2014)

Marchetti, M.C., Joanny, J.F., Ramaswamy, R., Liverpool, T.B., Prost, J., Rao, M., Aditi Simha, R.: Hydrodynamics of soft active matter. Rev. Mod. Phys. **85**, 1143 (2013)

Mussler, M., Rafaï, S., Peyla, P., Wagner, C.: Effective viscosity of non-gravitactic Chlamydomonas reinhardtii microswimmer suspensions. EPL **101**, 54004 (2013)

Rafaï, S., Jibuti, L., Peyla, P.: Effective viscosity of microswimmer suspensions. Phys. Rev. Lett. **104**, 098102 (2010)

Saintillan, D., Darve, E., Shaqfeh, E.S.G.: A smooth particle-mesh Ewald algorithm for Stokes suspension simulations: the sedimentation of rigid fibers. Phys. Fluids **17**, 033301 (2005)

Saintillan, D.: The dilute rheology of swimming suspensions: a simple kinetic model. Exp. Mech. **50**, 1275 (2010)

Saintillan, D., Shelley, M.J.: Orientational order and instabilities in suspensions of self-locomoting rods. Phys. Rev. Lett. **99**, 058102 (2007)

Saintillan, D., Shelley, M.J.: Instabilities and pattern formation in active particle suspensions: kinetic theory and continuum simulations. Phys. Rev. Lett. **100**, 178103 (2008)

Saintillan, D., Shelley, M.J.: Instabilities, pattern formation, and mixing in active suspensions. Phys. Fluids **20**, 123304 (2008)

Saintillan, D., Shelley, M.J.: Emergence of coherent structures and large-scale flows in motile suspensions. J. R. Soc. Interface **9**, 571 (2012)

Saintillan, D., Shelley, M.J.: Active suspensions and their nonlinear models. C. R. Physique **14**, 497 (2013)

Saintillan, D., Shelley, M.J.: Theory of active suspensions. In: Spagnolie, S.E. (ed.) Complex Fluids in Biological Systems: Experiment, Theory, and Computation, pp. 319–355. Springer, New York (2015)

Sanchez, T., Chen, D.T., DeCamp, S.J., Heymann, M., Dogic, Z.: Spontaneous motion in hierarchically assembled active matter. Nature **491**, 431 (2012)

Schaller, V., Weber, C., Semmrich, C., Frey, E., Bausch, A.R.: Polar patterns of driven filaments. Nature **467**, 73 (2010)

Sokolov, A., Aranson, I.S.: Reduction of viscosity in suspension of swimming bacteria. Phys. Rev. Lett. **103**, 148101 (2009)

Subramanian, G., Koch, D.L.: Critical bacterial concentration for the onset of collective swimming. J. Fluid Mech. **632**, 359 (2009)